Journal of Materials Chemistry

Cite this: *J. Mater. Chem.*, 2012, **22**, 8083

www.rsc.org/materials

PAPER

Polycondensation of thiourea into carbon nitride semiconductors as visible light photocatalysts†

Guigang Zhang, Jinshui Zhang, Mingwen Zhang and Xinchen Wang*

Received 5th January 2012, Accepted 27th February 2012
DOI: 10.1039/c2jm00097k

Converting solar energy into hydrogen gas by water splitting is considered as a long-term solution to address global energy and environmental problems. Great effort has been devoted to the search for abundant systems for the purpose of efficient capture, conversion, and storage of solar energy in a cost-effective manner. To further advance the recently-developed carbon nitride photocatalysis for solar hydrogen generation, thiourea, a sulfur-containing compound, was used as a cheap and easily-available starting material for the synthesis of graphitic carbon nitride semiconductors. The as-prepared photocatalysts were subjected to several characterizations, and the results showed that the heating temperature and the presence of sulfur motifs offer a facile chemical pathway for the control of the condensation/polymerization of carbon nitride, and thus adjusting their textural and electronic properties. Photocatalytic activity experiments demonstrated that the g-C_3N_4 synthesized from thiourea exhibited a much higher H_2 production rate than that of g-C_3N_4 prepared from dicyanamide or urea, and this activity can be further enhanced by increasing the condensation temperature.

1. Introduction

Catalytically splitting water by sunlight to produce hydrogen gas has attracted worldwide attention due to increasing energy demands and growing greenhouse gas emissions.[1] Since the discovery of H_2 production by water splitting in Pt/TiO_2 photoelectrochemical cells in 1972,[2] enormous efforts have been made to establish stable, efficient and affordable heterogeneous photocatalytic systems for solar to chemical conversion.[3] Various kinds of homogeneous and heterogeneous photocatalytic systems have been explored in the past few decades, based mostly on such solar energy transducers as metal oxides,[4] metal (oxy)nitrides,[5] metal (oxy)sulfides[6] and non-metal doped or plasma based TiO_2 photocatalysts.[7] However, the search for a non-toxic, low cost, but stable and efficient visible light photocatalyst remains a difficult challenge and is actively pursued nowadays.[8]

Graphitic carbon nitride (g-C_3N_4) polymers, the most stable allotrope of covalent carbon nitride solids at ambient conditions,[9] have been successfully introduced as a new metal-free visible light photocatalyst for water reduction and oxidation, owing to their unique electronic band structure.[10] To advance this sustainable photocatalytic material, many strategies have been adopted to modify its physical and chemical properties, such as doping,[11] sensitization,[12] nanostructured design,[13] and hybridization,[14] as well as copolymerization.[15] In addition, the use of different precursors that contain C≡N core structures for g-C_3N_4 synthesis has also been proven to be an effective means of enhancing the photocatalytic performance of g-C_3N_4. For example, g-C_3N_4 synthesized from dicyanodiamide (DCDA) showed a better photoactivity for methylene blue (MB) degradation than g-C_3N_4 synthesized from cyanamide (CA) and melamine (MA).[16] Using sulfur containing C≡N based compounds as the precursors for g-C_3N_4 preparation, such as trithiocyanuric acid (TA)[17] and ammonium thiocyanate (AT),[18] can alter the traditional way of monomer condensation/polymerization by the sulfur-mediated effect, optimizing its textural, optical and electronic properties for photoredox catalysis.

Very recently, urea, an oxygen-containing compound, has been thermally-transformed into polymeric g-C_3N_4.[19] The resultant photocatalyst showed enhanced photocatalytic reactivity for dye degradation under visible light irradiation, due mainly to the surface enlargement effect. The possible reaction mechanism for urea conversion into a g-C_3N_4 network at high temperatures is presented in Scheme 1, where oxygen compounds act as additional leaving motifs to facilitate the condensation of carbon nitride materials, and thus enable structural perfection.[19] What will happen if oxygen atoms are substituted by sulfur atoms? Do g-C_3N_4 networks still form when thiourea (TU) is used as the starting material, which has a similar molecular structure to urea, but with easy-leaving groups of sulfur species? In principle, TU can undergo self-polymerization and condensation at high temperature to form g-C_3N_4 networks (Scheme 1), whereas the sulfur species can promote the connectivity and

Research Institute of Photocatalysis, Fujian Provincial Key Laboratory of Photocatalysis-State Key Laboratory Breeding Base, Fuzhou University, Fuzhou 350002, People's Republic of China. E-mail: xcwang@fzu.edu.cn

† Electronic supplementary information (ESI) available: characterization of XRD, FT-IR and UV-Vis spectra for CN-U samples; EPR spectra for bulk and mpg-C_3N_4 samples. See DOI: 10.1039/c2jm00097k

packing of g-C_3N_4 sheets, as already known in the TA condensation scheme.[17] It is reported that a melon structure has been obtained at low temperature (400 °C) by using TU as the starting material, with the aid of TiO_2 or SiO_2.[20] However, the very low degree of polymerization and the incomplete formation of an electronic band structure impart the carbon nitride polymers with very moderate performances in photocatalytic applications.[20] Thus, the synthesis of well-condensed g-C_3N_4 photocatalysts from TU is still necessary, especially without the aid of inorganic substrates to support polymerization/condensation, while also taking advantage of a sulfur-mediated synthesis using easily available TU instead of TA to promote bulk condensation kinetically.

In this paper, TU was used as a single precursor for g-C_3N_4 synthesis at different temperatures. The textural structures, optical and electronic properties of the resultant samples were carefully examined. The TU-derived g-C_3N_4 photocatalysts were applied in solar hydrogen production, and the performance was compared with other g-C_3N_4 solids obtained from conventional starting materials, such as DCDA and urea.

2. Experimental

2.1. Preparation of g-C_3N_4

g-C_3N_4 photocatalysts were prepared by directly heating TU at different temperatures for 2 h in air, and the resultant samples were denoted as CN-T_x, where x refers to the calcination temperature. For comparison, DCDA and urea were also used as the starting materials for carbon nitride synthesis under the same preparation conditions, and the obtained samples were denoted as CN-D_x and CN-U_x, respectively.

2.2. Characterization

Powder X-ray diffraction (XRD) measurements were performed on a Bruker D8 Advance diffractometer with Cu-Kα1 radiation ($\lambda = 1.5406$ Å). Fourier transform infrared (FTIR) spectra were recorded on a BioRad FTS 6000 spectrometer. X-Ray photoelectron spectroscopy (XPS) data were obtained on a Thermo ESCALAB250 instrument with a monochromatized Al Kα line source (200 W). Nitrogen adsorption–desorption isotherms were collected at 77 K using a Micromeritics ASAP 2020 surface area and porosity analyzer. Transmission electron microscopy (TEM) was performed by a Zeiss 912 microscope and a JEOL mode JEM 2010 EX instrument. Electron paramagnetic resonance (EPR) measurements were carried out on a Bruker model A300 spectrometer. UV-Vis diffuse reflectance spectra (DRS) were performed on a Varian Cary 500 Scan UV-visible system. Photoluminescence spectra were recorded on a Edinburgh FI/FSTCSPC 920 spectrophotometer. Elemental analysis (EA) results were collected from a Vario MICRO. TGA was performed on a TG209 (NETZSCH Co.). Electrochemical measurements were conducted with a BAS Epsilon Electrochemical System in a conventional three electrode cell, using a Pt plate as the counter electrode and an Ag/AgCl electrode (3 M KCl) as the reference electrode.

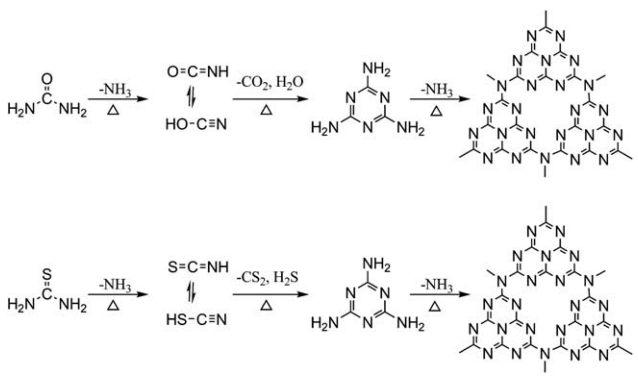

Scheme 1 The self-polymerization of urea and thiourea into a graphitic carbon nitride network at high temperatures.

2.3. Photocatalytic activity for hydrogen evolution

Reactions were carried out in a Pyrex top-irradiation reaction vessel connected to a glass closed gas system. H_2 production was performed by dispersing 50 mg of catalyst powder in an aqueous solution (100 mL) containing triethanolamine (10 vol%) as a sacrificial electron donor. 3 wt% Pt was loaded on the surface of the carbon nitride catalyst by the *in situ* photodeposition method using H_2PtCl_6. The reaction solution was evacuated several times to remove air completely prior to irradiation under a 300 W xenon-lamp and a water filter. The wavelength of the incident light was controlled by applying appropriate long-pass cut-off filters. The temperature of the reaction solution was maintained at room temperature by the flow of cooling water during the reaction. The evolved gases were analyzed by gas chromatography equipped with a thermal conductive detector (TCD) and a 5 Å molecular sieve column, using argon as the carrier gas.

Details for Pt *in situ* loading: 100 μL of H_2PtCl_6 aqueous solution (Sigma-Aldrich, 0.015 g mL^{-1} based on Pt) was added to the reaction solution (100 mL) containing 50 mg g-C_3N_4 and 10 vol% triethanolamine. The reaction system was then closed and the solution was evacuated 10 times to remove the air completely. A Xe-lamp equipped with IR and 420 nm filters was turned on to induce the *in situ* photodeposition of Pt particles on the carbon nitride polymers.

3. Results and discussion

3.1. Formation of g-C_3N_4

To demonstrate the formation of well condensed graphitic-like conjugated aromatic systems and the complete development of semiconductor band structures, the as-prepared CN-T_{550}, together with CN-D_{550} and CN-U_{550} as the references, was subjected to several characterizations, such as XRD, FT-IR, XPS, N_2-sorption, TEM and EPR. In addition, the differences in the textural structure, optical and electronic properties between CN-T_{550} and the reference samples were also discussed.

In Fig. 1a, highly graphitic-like structures are observed for CN-T_{550} and the reference samples, suggesting the formation of a well-developed C_3N_4 layer structure.[9] The strongest XRD peak, originating from the (002) interlayer reflection of a graphitic-like structure, is determined as 27.4°, corresponding to an interlayer distance of $d = 0.326$ nm. This interlayer distance is almost the same as that of CN-D_{550}, but is slightly smaller than

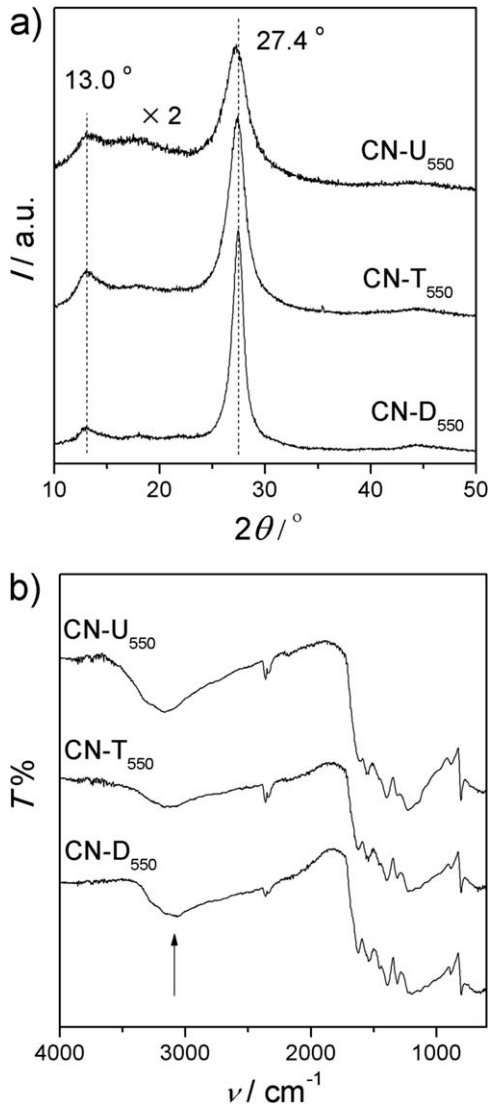

Fig. 1 XRD patterns (a) and FT-IR (b) spectra of CN-U_{550}, CN-T_{550} and CN-D_{550}.

that of CN-U_{550} (d = 0.328 nm).[18] In the case of the other pronounced XRD peak at *ca.* 13.0°, related to in-plane repeated units, no obvious difference can be detected among the samples of CN-T_{550}, CN-D_{550} and CN-U_{550}. This indicates that the three samples possess virtually the same void-to-void distance (d = 0.681 nm) of the in-plane structural repeating motifs.[9,18] In addition, the intensity of the XRD patterns is found to be different from each other depending on the starting materials. The XRD peak of CN-T_{550} is found to be less strong than that of CN-D_{550}, but it is stronger and sharper than that of CN-U_{550}. We attribute the weak and broad XRD peaks of CN-U_{550} to the disturbance of the graphitic-like structure, which is related to its enlarged surface area and the presence of nanostructures (Fig. 3).[15,18]

Fig. 1b shows the FT-IR spectra of the three samples. All of the characteristic vibration modes assigned to typical g-C_3N_4 are clearly seen for CN-T_{550}, indicating the successful evolution of the g-C_3N_4 structure.[9] The strong bands at 1200–1600 cm^{-1} are assigned to the stretching vibration of the heptazine heterocyclic ring (C_6N_7) units, while the sharp peak at 805 cm^{-1} is considered as their breathing mode.[15] The broad peak located at 2900–3300 cm^{-1} is attributed to the residual N–H components and the O–H bands, associated with the uncondensed amino groups and the absorbed H_2O molecules, respectively. The CN-T_{550} sample is observed to present a lower intensity of the broad band at 2900–3300 cm^{-1} than both the CN-D_{550} and CN-U_{550} samples, indicating the accelerated and improved condensation of g-C_3N_4 through the sulfur-mediated synthesis.[17,18] The weak absorption at 2350 cm^{-1} is due to absorbed CO_2 molecules on the g-C_3N_4 surface.[21]

The chemical structure and composition of CN-T_{550} were further revealed by XPS measurements. In the XPS survey spectrum, as shown in Fig. 2a, there are only three elements (C, N, and O) observed. No signal assigned to the sulfur species can be found, which is similar to the results for AT-derived g-C_3N_4. This gives evidence that the function of the sulfur species in these CN precursors is to mediate the g-C_3N_4 condensation/polymerization instead of to dope/modify the carbon nitride semiconductors.[17,18] The O 1s signal is presumably due to the absorbed H_2O or CO_2 molecules on the CN-T_{550} surface, as also confirmed by the above FT-IR analysis (Fig. 1b).[18] High-resolution spectra of C 1s, N 1s and S 2p are also shown in Fig. 2. There are mainly two carbon species present in the C 1s spectrum, and the corresponding binding energies are determined to be 284.6 eV and 288.1 eV. The former peak, according to the literature, is typically ascribed to sp^2 C–C bonds, whereas the latter is identified as sp^2-bonded carbon in N-containing aromatic rings (N–C=N), which is regarded as the major carbon species in the g-C_3N_4 polymer.[9] The N 1s spectrum can be deconvoluted into four peaks at 398.7 eV, 400.3 eV, 401.4 eV and 404.2 eV. The main peak centered at 398.7 eV originates from the

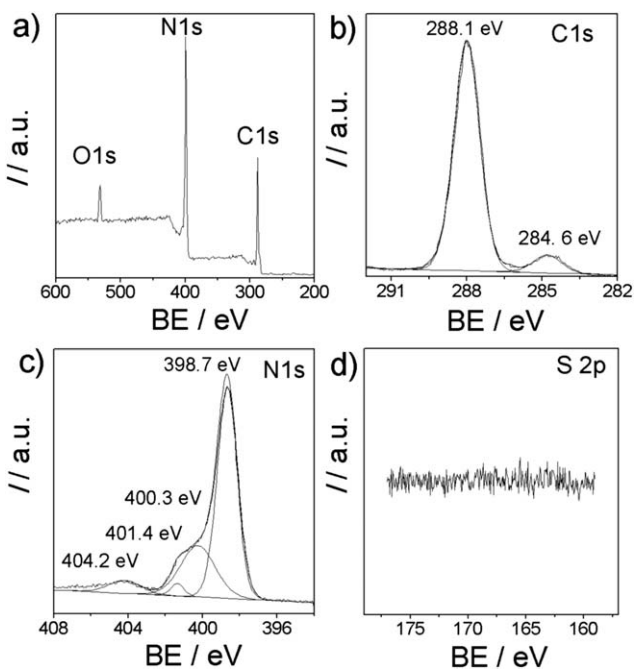

Fig. 2 XPS survey spectrum (a) and the corresponding high-resolution spectra of C1s (b), N1s (c), S2p (d) that are obtained from the CN-T_{550} sample.

sp^2-bonded N involved in the triazine rings (C–N=C), while the weak peak at 400.3 eV is caused by the tertiary nitrogen N–$(C)_3$ groups. Both of them, together with sp^2 C (N–C=N), make up the heptazine heterocyclic ring (C_6N_7) units, constructing the basic substructure units of the g-C_3N_4 polymers. Another weak peak at 401.4 eV indicates the presence of amino functions (C–N–H), originating from the defective condensation of melon structures. In addition, the peak at 404.2 eV is attributed to the charging effects or positive charge localization in the heterocycles.[9] Note again that there is no signal attributed to S 2p ($2p_{3/2}$ = 164.0 eV) species, even at the carefully-repeated scanning spectrum of S 2p in high-resolution, consistent with the elemental analysis results.

It is noted that the textural structure of the final g-C_3N_4 polymers is strongly dependant on the different C≡N based precursors used. For example, the urea-derived g-C_3N_4 possesses a large surface area (~58 $m^2\ g^{-1}$ for CN-U_{550}).[19] However, in the case of thiourea, the specific surface area (S_{BET}) of CN-T_{550} is determined as 18 $m^2\ g^{-1}$, according to the nitrogen adsorption–desorption experiments, as shown in Fig. 3. This indicates that the heteroatoms, oxygen and sulfur, play a very important role in the processing of carbon nitride condensation, and oxygen is found to be more efficient for enlarging the surface area of g-C_3N_4, presumably due to the formation of CO_2 during the polymerization to inhibit grain advance by chemisorption at basic docking sites. The S_{BET} of CN-D_{550} was measured as 10 $m^2\ g^{-1}$.

Fig. 4 shows the typical TEM images of CN-D_{550}, CN-T_{550} and CN-U_{550}, respectively. Similar to the results of the nitrogen adsorption–desorption experiments, the starting materials also have a significant influence on the morphological evolution of the terminal g-C_3N_4 samples. CN-D_{550} is mainly composed of large particles and sheets, whereas much smaller sizes of particles and sheets are clearly observed for the CN-T_{550} sample. The morphology of CN-U_{550} was quite different, and many smooth, thin and flat layers were clearly seen in Fig. 4c. This typical silk-like morphology imparts CN-U_{550} with a large specific surface area, as demonstrated previously.

Room-temperature EPR analysis was carried out to investigate the electronic band structure of the g-C_3N_4 polymers. In Fig. 5, only one single Lorentzian line centered at a g value of 2.0034 is observed for all of the g-C_3N_4 samples, indicating the

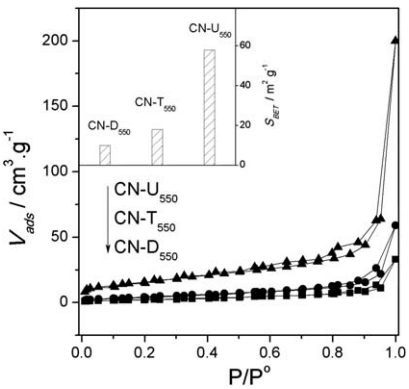

Fig. 3 N_2 adsorption–desorption isotherms and the corresponding specific surface area (inset) of CN-D_{550}, CN-T_{550} and CN-U_{550}.

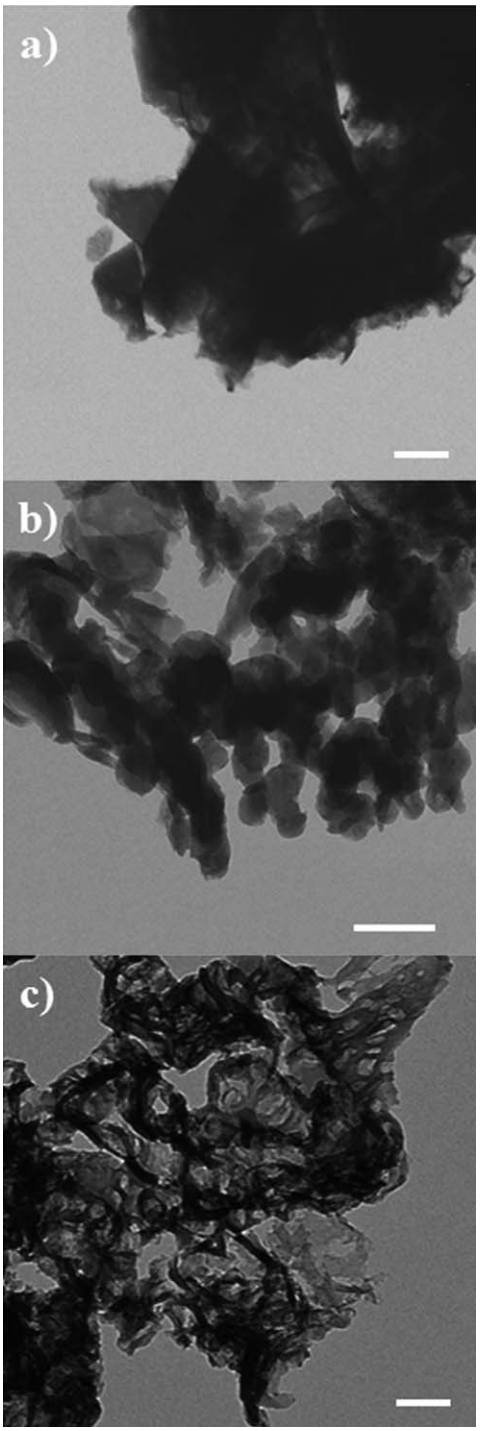

Fig. 4 Typical TEM images of CN-D_{550} (a), CN-T_{550} (b) and CN-U_{550} (c), respectively. The scale bars are 200 nm.

establishment of a semiconductor structure at 550 °C in the three samples. These Lorentzian lines, according to the literature, originate from the unpaired electrons in the aromatic rings of carbon atoms, within the π-bonded nanosized clusters on the surface of the materials.[15b,22] In addition, the intensity of the Lorentzian lines is quite different, obeying a linear correlation with the corresponding surface area of the samples (Fig. 5b). A similar conclusion can also be derived for mpg-C_3N_4 and bulk

g-C_3N_4 synthesized from cyanamide (Fig. S2†). mpg-C_3N_4 with a large surface area (128 $m^2\ g^{-1}$) exhibits a stronger Lorentzian line than bulk g-C_3N_4 (S_{BET} = 11 $m^2\ g^{-1}$), consistent with the density of surface sites.

3.2. Influence of heat treatment

In the following set of experiments, we focus on the influence of heating temperature on the textural structure, optical and electronic properties of CN-T_x.

Fig. 6a shows the XRD patterns of the TU-derived carbon nitride samples condensed at different heating temperatures. It can be seen that at 450 °C, graphitic-like networks are formed but are incomplete, because the reaction temperature is too low to provide enough energy for thiourea condensation. Upon increasing the temperature to 500 °C, typical graphitic-like layered structures form, with the appearance of a (002) and (100) peak in the XRD patterns. Further increasing the temperature to 550 and 600 °C can optimize the polycondensation of g-C_3N_4, but excessive thermal energy at 650 °C can induce the decomposition of the carbon nitride polymer (Fig. 7c).[18,19] For example, when the reaction temperature reaches 650 °C, the (002) peak up-shifts to $2\theta = 27.9°$, resulting in a more compact g-C_3N_4 with an interlayer distance of d = 0.320 nm. Further increasing the temperature to 700 °C causes the completely combustion of g-C_3N_4 in air.

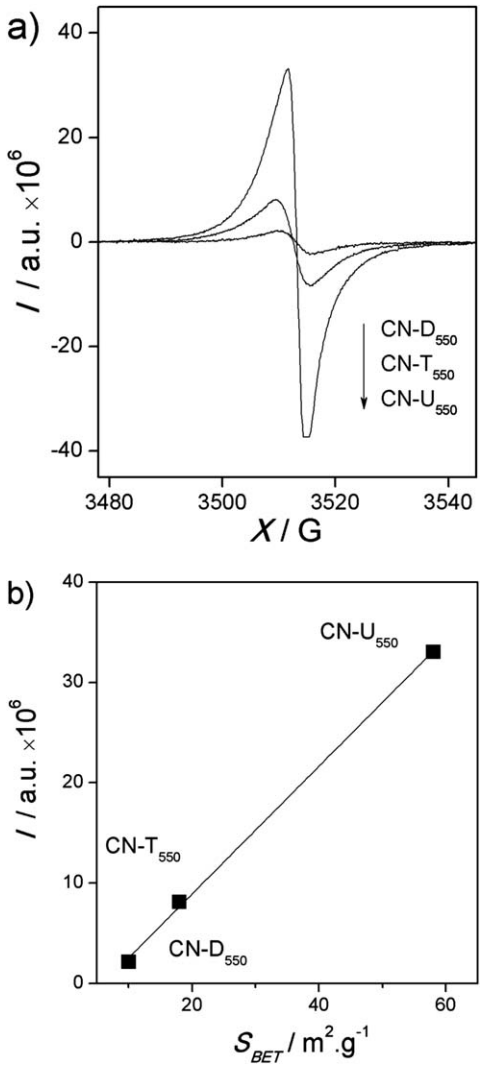

Fig. 5 EPR signals (a) and the correlation between S_{BET} and the peak intensity (b) of CN-D_{550}, CN-T_{550} and CN-U_{550} at room temperature.

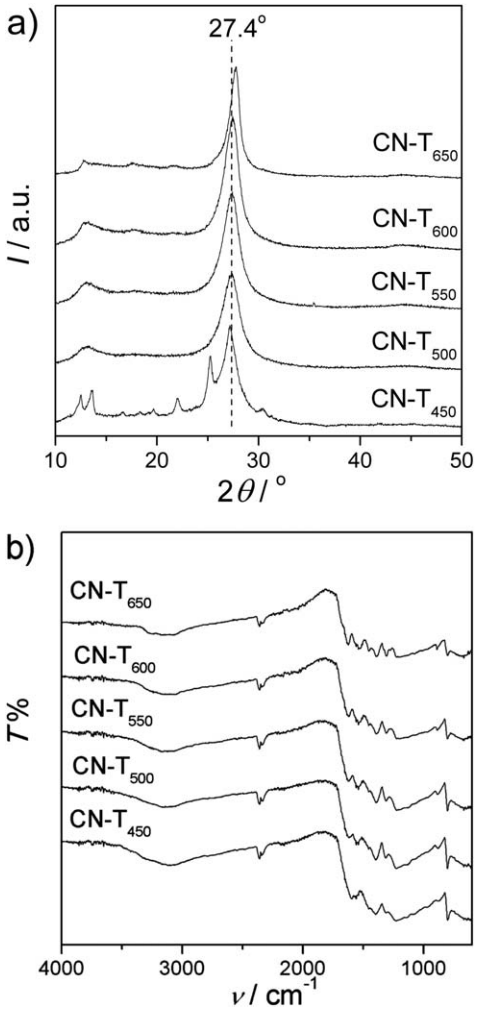

Fig. 6 XRD patterns (a) and FT-IR spectra (b) of the CN-T_x samples.

A similar structural evolution trend can be inferred from the FT-IR spectra (Fig. 6b) of the samples prepared at different temperatures. At low temperatures, such as 450 °C, the incomplete condensation of thiourea results in the weak vibration of the C_6N_7 units at 1200 to 1600 cm^{-1} and 805 cm^{-1}, with a quite strong signal for residual N–H components from 2900 cm^{-1} to 3300 cm^{-1}. This poor condensation can be improved by increasing the heating temperature to promote the process of g-C_3N_4 formation. However, the rate of sample self-decomposition accelerates at the same time, when the sample was subjected to sintering at >650 °C.

Fig. 7 shows the N_2-sorption analysis and the corresponding surface area of g-C_3N_4 synthesized at different temperatures, together with the thermal analysis of the g-C_3N_4 in air. When the heating temperature exceeds 550 °C, above the onset decomposition temperature of the g-C_3N_4 polymers, the weight loss happens quickly, accompanied by the significant

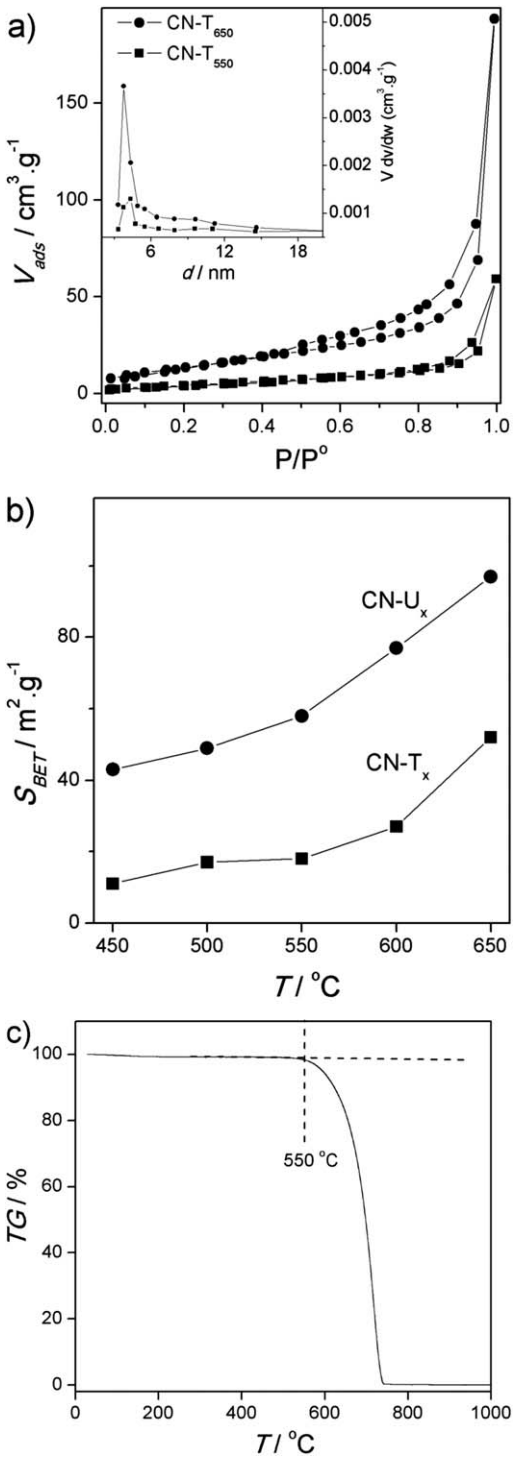

Fig. 7 (a) N_2 adsorption–desorption isotherms and the corresponding BJH pore-size distribution (inset) of CN-T_{550} and CN-T_{650}. (b) The correlation between S_{BET} and the heating temperature for CN-T_x and CN-U_x. (c) Thermogravimetric analysis (TGA) results for CN-T_{600}.

enlargement of S_{BET} and the generation of nanopores (Fig. 7 and Table 1). For example, increasing the condensation temperature from 550 °C to 650 °C causes a great enhancement of the specific surface area from 18 $m^2\ g^{-1}$ for CN-T_{550} to 52 $m^2\ g^{-1}$ for CN-T_{650}.

TEM images provide us with clear evidence of the thermal decomposition behavior (Fig. 4b and Fig. 8). In comparison to CN-T_{550}, g-C_3N_4 sheets with much smaller particle sizes are visible in the 650 °C condensed sample (CN-T_{650}), owing to the serious decomposition of g-C_3N_4 in the presence of oxygen. This thermal behavior of the carbon nitride photocatalysts is contrary to most porous inorganic photocatalysts, which typically undergo structure deformation/collapse with decreased surface area upon enhancing the sintering temperature to improve crystal growth. However, it is observed that for carbon nitride organosemiconductors, the nanostructure can be self-introduced by a simple thermal treatment. This is a remarkable observation, as the creation of porous structures in the polymeric carbon nitride frameworks typically relies on complicated hard-templating methods using nanosized SiO_2 particles and mesoporous SBA-type zeolites to support the polymerization of the carbon nitride precursors, followed by the careful removal of the templates with HF or NH_4HF_2.[9,13] The slight thermal decomposition will also create surface sites to facilitate catalytic sorption and also to promote the localization of light-induced electrons in the conjugated systems, which has already been demonstrated to be beneficial for carbon nitride photocatalysis.[13a,b]

The relationship between the optical properties and the heating temperatures is examined by UV-vis and photoluminescence (PL) spectra. In Fig. 9, a typical semiconductor absorption in the blue light range is observed for all CN-T_x samples, which originates from electronic transitions from the VB to the CB.[10] Their absorption edges are varied by changing the calcination temperature. Firstly, with increasing the temperature from 450 °C to 550 °C, an obviously reduced band gap energy from 2.71 eV to 2.58 eV is detected (Table 1), owing to the extension of electron delocalization in the aromatic sheets with enhanced structural connections, somewhat similar to the bathochromic shift effect in J-aggregates.[13,18] Further increasing the condensation temperature causes the slight blue-shift of the absorption edges, for instance, a bigger band gap of 2.76 eV is determined for CN-T_{650}. This hypsochromic-shift performance is presumably due to the strong quantum confinement effects, because high temperatures can induce the thermal decomposition of g-C_3N_4 into smaller particles (Fig. 7 and 8). However, the H-aggregates inducing a hypsochromic-shift in the optical spectrum following the improved condensation at 650 °C cannot be exclusively ruled out, because the layer structure is indeed found to be compressed to a smaller inter-plane distance from $d = 0.326$ nm (550 °C) to $d = 0.320$ nm (650 °C).

Fig. 10 gives the PL spectra of different samples, showing that the PL intensity increases with increasing temperature from 450 °C to 500 °C, due to the gradual formation of a semiconductor band structure. The PL spectra become broader and less intense with further increased heating temperature, because the presence of thermally-induced nanostructures (Fig. 7) can cause the electron relocalization on surface terminal sites, which is believed to promote photocatalytic redox functions.[13a,b]

The charge generation and separation within g-C_3N_4/water interfaces (similar to semiconductor/electrolyte interfaces, SEI) is the basic process for photocatalytic water splitting. The photoelectrochemistry setup provides a simple but powerful tool to monitor this process.[15] Powder catalysts are made as film

Table 1 Physicochemical properties and photocatalytic activity of g-C_3N_4 polymers for H_2 evolution with visible light

Catalyst	C/N atomic	S_{BET}[a]/m^2 g^{-1}	Band gap[b]/eV	HER[c]/μmol h^{-1}
CN-D_{550}	0.73	10	2.75	12.1
CN-T_{450}	0.66	11	2.71	5.7
CN-T_{500}	0.68	17	2.70	30.3
CN-T_{550}	0.70	18	2.58	90.7
CN-T_{600}	0.72	27	2.62	151.1
CN-T_{650}	0.76	52	2.76	157.2
CN-U_{450}	0.78	43	2.79	3.4
CN-U_{500}	0.76	49	2.70	23.5
CN-U_{550}	0.76	58	2.66	79.0
CN-U_{600}	0.75	77	2.67	109.1
CN-U_{650}	0.73	97	2.69	89.8

[a] Calculated from nitrogen adsorption–desorption isotherms. [b] Estimated from optical measurements. [c] H_2 evolution rate.

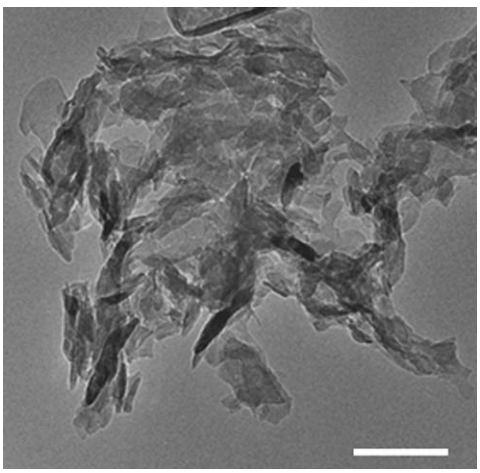

Fig. 8 Typical TEM image of CN-T_{650}. The scale bar is 200 nm.

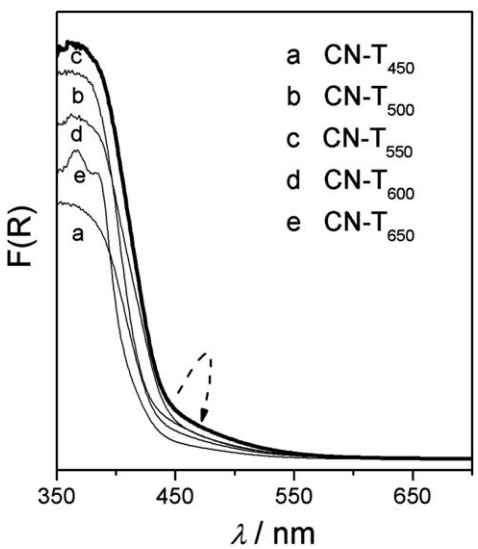

Fig. 9 UV-vis spectra of the CN-T_x samples.

electrodes on fluorine doped tin oxide (FTO) glass by a drop-coating method. Then, these film electrodes are immersed into a 0.2 M Na_2SO_4 electrolyte, under visible light (λ > 420 nm) illumination to generate photocurrents. As shown in Fig. 11,

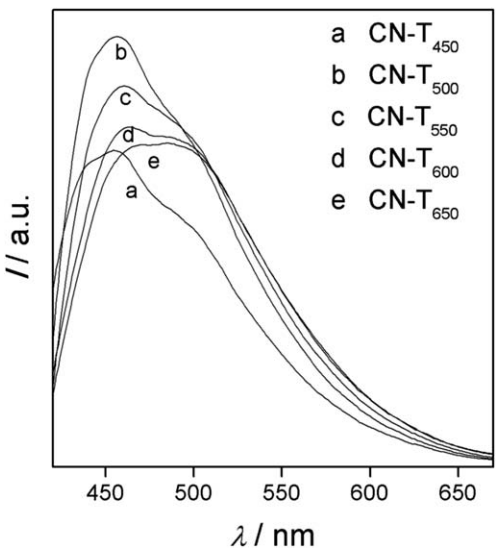

Fig. 10 Photoluminescence spectra under 400 nm excitation at 298 K for the CN-T_x samples.

obvious anodic photocurrents are generated by the g-C_3N_4 photoelectrodes at 0.4 V *vs.* Ag/AgCl, indicating the efficient generation and separation of photoinduced electron–hole pairs within the SEI. CN-T_{650} produces a bigger photocurrent than CN-T_{550}, owing to its better condensation and enlarged surface area, which is favorable for charge collection and separation at the interfaces.

3.3. Photocatalytic activity

The photocatalytic activity of the resulting g-C_3N_4 samples was evaluated by H_2 production from aqueous proton solution under visible light irradiation (λ > 420 nm). Chloroplatinic acid and triethanolamine were used as precursors to create H_2 reduction sites (Pt nanoparticles) and electron donors, respectively. CN-T_{550} (with a catalytic performance of 90.7 μmol h^{-1}) shows the best H_2 evolution activity over the samples of CN-U_{550} (79.0 μmol h^{-1}) and CN-D_{550} (12.1 μmol h^{-1}), albeit a larger S_{BET} was detected for CN-U_{550} and a better crystallinity was observed for CN-D_{550} (Table 1). The H_2 evolution activities of the other CN-T_x and CN-U_x samples are also summarized in Table 1. Not

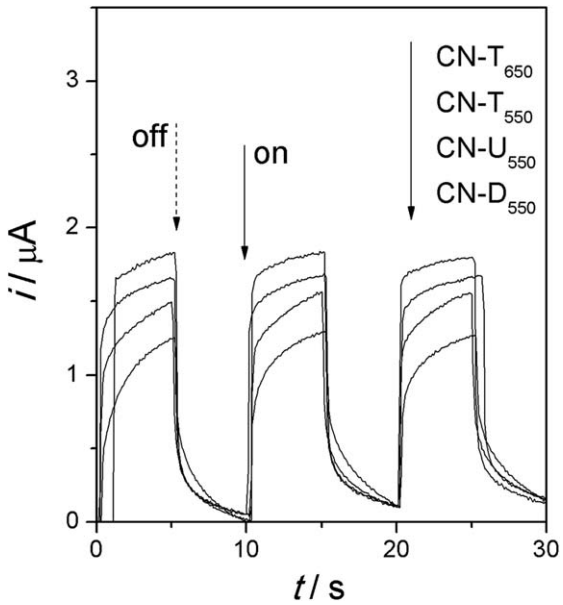

Fig. 11 Transient photocurrent generation from g-C_3N_4/FTO electrodes at 0.4 V *vs.* Ag/AgCl in 0.2 M Na_2SO_4 under visible light irradiation ($\lambda > 420$ nm). The active surface area of the film electrode was controlled as 0.25 cm^2.

unexpectedly, their activities varied greatly with heating temperature, again reflecting the importance of heat treatment for photocatalyst synthesis.

Fig. 12a shows the time course of H_2 evolution obtained over the CN-T_{650} sample under visible light ($\lambda > 420$ nm) irradiation. The production of H_2 increases steadily with prolonged time of light irradiation. After four consecutive runs (12 h), a total of 1.1 mmol H_2 gas (24.6 mL) is produced, and no obvious deactivation of the photocatalysts is found, suggesting the good stability of CN-T_{650} as an organic photocatalyst for solar H_2 generation. This is very important, because good stability is regarded as a crucial basis for a photocatalyst for solar energy application.

To further confirm that water reduction is indeed driven by visible absorption by the carbon nitride catalyst, a wavelength-dependent H_2 evolution experiment was also performed. In Fig. 12, the trend of H_2 production matches well with the UV-vis spectrum of CN-T_{650}, and the longest wavelength available for H_2 evolution is about 550 nm. This observation strongly supports that the water reduction process is primarily induced by light-excitation of electrons in the carbon nitride polymer.

4. Conclusions

In summary, g-C_3N_4 photocatalysts have been successfully synthesized from thiourea at different temperatures in air. The presence of the sulfur species offers an extra chemical control for the synthesis of graphitic carbon nitride networks, accelerating the processing of the g-C_3N_4 polymerization/condensation. In addition, the condensation temperature was found to affect the formation of g-C_3N_4 greatly. Increasing the heating temperature to 650 °C not only favors the g-C_3N_4 formation, but also accelerates the partial decomposition of the catalyst itself, *in situ*, creating nanostructures in the bulk carbon nitrides. Therefore, one can easily optimize the textural, electronic and optical properties of carbon nitride semiconductors by the combination of a sulfur-mediated synthesis and the thermally-induced generation of nanostructures. These optimized g-C_3N_4 photocatalysts can, in principle, be implemented in other applications of catalysis and photocatalysis, such as selective organic photosynthesis and environmental protection.[23]

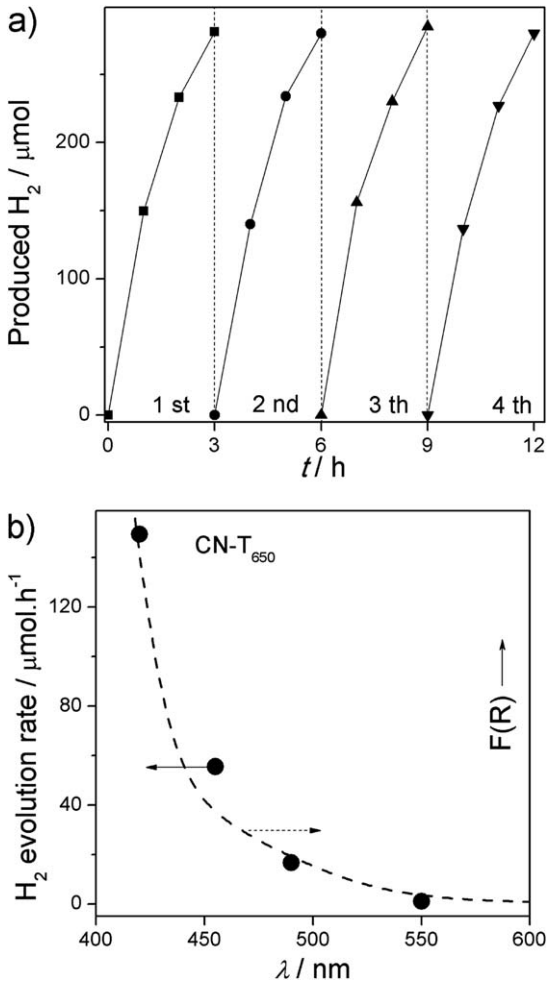

Fig. 12 (a) Time course of H_2 evolution for CN-T_{650} under visible light irradiation ($\lambda > 420$ nm). (b) Wavelength dependence of H_2 evolution rate on CN-T_{650}, the dashed line is the UV-vis spectra of CN-T_{650}.

Acknowledgements

This work is financially supported by the National Natural Science Foundation of China (21033003 and 21173043). The authors thank Dr M. J. Bojdys for the helpful discussions.

Notes and references

1 (*a*) R. M. Navarro, M. A. Peña and J. L. G. Fierro, *Chem. Rev.*, 2007, **107**, 3952; (*b*) A. W. Hains, Z. Q. Liang, M. A. Woodhouse and B. A. Gregg, *Chem. Rev.*, 2010, **110**, 6689; (*c*) A. I. Hochbaum and P. D. Yang, *Chem. Rev.*, 2010, **110**, 527; (*d*) X. B. Chen, S. H. Shen, L. J. Guo and S. S. Mao, *Chem. Rev.*, 2010, **110**, 6503; (*e*) A. Kudo and Y. Miseki, *Chem. Soc. Rev.*, 2009, **38**, 253; (*f*) Frank

E. Osterloh, *Chem. Mater.*, 2008, **20**, 35; (*g*) K. Maeda and K. Domen, *J. Phys. Chem. C*, 2007, **111**, 7851.
2 A. Fujiashima and K. Honda, *Nature*, 1972, **238**, 37.
3 (*a*) K. Maeda, K. Teramura, D. Lu, T. Takata, N. Saito, Y. Inoue and K. Domen, *Nature*, 2006, **440**, 295; (*b*) M. G. Schwab, M. Hamburger, X. L. Feng, J. Shu, H. W. Spiess, X. C. Wang, M. Antoniettib and K. Mullen, *Chem. Commun.*, 2010, **46**, 8932; (*c*) T. F. Yeh, J. M. Syu, C. Cheng, T. H. Chang and H. Teng, *Adv. Funct. Mater.*, 2010, **20**, 2255; (*d*) L. Zhao, X. F. Chen, X. C. Wang, Y. J. Zhang, W. Wei, Y. H. Sun, M. Antonietti and M. Titirici, *Adv. Mater.*, 2010, **22**, 3317.
4 (*a*) R. Asahi, T. Morikawa, T. Ohwaki, K. Aoki and Y. Taga, *Science*, 2001, **293**, 269; (*b*) Z. Zou, J. Ye, K. Sayama and H. Arakawa, *Nature*, 2001, **414**, 625; (*c*) Y. Hosogi, K. Tanabe, H. Kato, H. Kobayashi and A. Kudo, *Chem. Lett.*, 2004, **33**, 28; (*d*) H. G. Kim, D. W. Hwang and J. S. Lee, *J. Am. Chem. Soc.*, 2004, **126**, 8912.
5 (*a*) K. Maeda, K. Teramura, D. L. Lu, T. Takata, N. Saito, Y. Inoue and K. Domen, *Nature*, 2006, **440**, 295; (*b*) K. Maeda and K. Domen, *MRS Bull.*, 2010, **36**, 25; (*c*) K. Maeda, T. Takata, M. Hara, N. Saito, Y. Inoue, H. Kobayashi and K. Domen, *J. Am. Chem. Soc.*, 2005, **127**, 8286.
6 (*a*) A. Kudo and Y. Miseki, *Chem. Soc. Rev.*, 2009, **38**, 253; (*b*) I. Tsuji, H. Kato, H. Kobayashi and A. Kudo, *J. Am. Chem. Soc.*, 2004, **126**, 13406.
7 (*a*) T. Ohwaki, K. Aoki and Y. Taga, *Science*, 2001, **293**, 269; (*b*) S. U. M. Khan, M. Al-Shahry and W. B. Ingler Jr, *Science*, 2002, **297**, 2243; (*c*) T. Umebayashi, T. Yamaki, H. Itoh and K. Asai, *Appl. Phys. Lett.*, 2004, **81**, 454; (*d*) T. Umebayashi, T. Yamaki, H. Itoh and K. Asai, *Appl. Phys. Lett.*, 2002, **81**, 454; (*e*) D. M. Chen, Z. Y. Jiang, J. Q. Geng, Q. Wang and D. Yang, *Ind. Eng. Chem. Res.*, 2007, **46**, 2741; (*f*) X. F. Chen, X. C. Wang, Y. D. Hou, J. H. Huang, L. Wu and X. Z. Fu, *J. Catal.*, 2008, **255**, 59.
8 K. Maeda and K. Domen, *J. Phys. Chem. Lett.*, 2010, **1**, 2655.
9 (*a*) A. Thomas, A. Fischer, F. Goettmann, M. Antonietti, J. O. Müller, R. Schlögl and J. M. Carlsson, *J. Mater. Chem.*, 2008, **18**, 4893; (*b*) Y. Wang, X. C. Wang and M. Antonietti, *Angew. Chem., Int. Ed.*, 2011, **50**, 2; (*c*) D. S. Su, J. Zhang, B. Frank, A. Thomas, X. C. Wang, J. Paraknowitsch and R. Schlögl, *ChemSusChem*, 2010, **3**, 169; (*d*) A. Vinu, *Adv. Funct. Mater.*, 2008, **18**, 816; (*e*) A. Vinu, K. Ariga, T. Mori, D. Golberg, Y. Bando, T. Nakanishi and S. Hishita, *Adv. Mater.*, 2005, **17**, 1648; (*f*) A. Vinu, P. Srinivasu, D. P. Sawant, T. Mori, K. Ariga, J. S. Chang, S. H. Jhung, Y. K. Hwang and V. V. Balasubramanian, *Chem. Mater.*, 2007, **19**, 4367.
10 (*a*) X. C. Wang, K. Maeda, A. Thomas, K. Takanabe, G. Xin, J. M. Carlsson, K. Domen and M. Antonietti, *Nat. Mater.*, 2009, **8**, 76; (*b*) K. Maeda, X. C. Wang, Y. Nishihara, D. Lu, M. Antonietti and K. Domen, *J. Phys. Chem. C*, 2009, **113**, 4940.
11 (*a*) X. F. Chen, J. S. Zhang, X. Z. Fu, M. Antonietti and X. C. Wang, *J. Am. Chem. Soc.*, 2009, **131**, 11658; (*b*) X. C. Wang, X. F. Chen, A. Thomas, X. Z. Fu and M. Antonietti, *Adv. Mater.*, 2009, **21**, 1609; (*c*) G. Liu, P. Niu, C. H. Sun, S. C. Smith, Z. G. Chen, G. Q. Lu and H. M. Cheng, *J. Am. Chem. Soc.*, 2010, **132**, 11642; (*d*) Z. X. Ding, X. F. Chen, M. Antonietti and X. C. Wang, *ChemSusChem*, 2011, **4**, 274.
12 K. Takanabe, K. Kamata, X. C. Wang, M. Antonietti, J. Kubota and K. Domen, *Phys. Chem. Chem. Phys.*, 2010, **12**, 13020.
13 (*a*) X. C. Wang, K. Maeda, X. F. Chen, K. Takanabe and K. Domen, *J. Am. Chem. Soc.*, 2009, **131**, 1680; (*b*) X. F. Chen, Y. S. Jun, K. Takanabe, K. Maeda, K. Domen, X. Z. Fu, M. Antonietti and X. C. Wang, *Chem. Mater.*, 2009, **21**, 4093; (*c*) E. Z. Lee, Y. S. Jun, W. H. Hong, A. Thomas and M. M. Jin, *Angew.Chem., Int. Ed.*, 2010, **49**, 9706; (*d*) X. H. Li, J. S. Zhang, X. F. Chen, A. Fischer, A. Thomas, M. Antonietti and X. C. Wang, *Chem. Mater.*, 2011, **23**, 4344; (*e*) K. Kailasam, J. D. Epping, A. Thomas, S. Losse and H. Junge, *Energy Environ. Sci.*, 2011, **4**, 4668.
14 (*a*) G. Q. Li, N. Yang, W. L. Wang and W. F. Zhang, *J. Phys. Chem. C*, 2009, **113**, 14829; (*b*) T. P. Ang, *Catal. Commun.*, 2009, **10**, 1920; (*c*) S. C. Yan, S. B. Lv, Z. S. Li and Z. G. Zou, *Dalton Trans.*, 2010, **39**, 1488; (*d*) Y. Di, X. C. Wang, A. Thomas and M. Antonietti, *ChemCatChem*, 2010, **2**, 834; (*e*) J. S. Zhang, M. Grzelczak, Y. D. Hou, K. Maeda, K. Domen, X. Z. Fu, M. Antonietti and X. C. Wang, *Chem. Sci.*, 2012, **3**, 443.
15 (*a*) J. S. Zhang, X. F. Chen, K. Takanabe, K. Maeda, K. Domen, J. D. Epping, X. Z. Fu, M. Antonietti and X. C. Wang, *Angew. Chem., Int. Ed.*, 2010, **49**, 441; (*b*) J. S. Zhang, G. G. Zhang, X. F. Chen, S. Lin, L. Möhlmann, G. Dolega, G. Lipner, M. Antonietti, S. Blechert and X. C. Wang, *Angew. Chem., Int. Ed.*, 2012, DOI: 10.1002/anie.201106656.
16 Y. L. Meng, G. Xin and D. Chen, *OAM-RC.*, 2011, **5**, 648.
17 J. S. Zhang, J. H. Sun, K. Maeda, K. Domen, P. Liu, M. Antonietti, X. Z. Fu and X. C. Wang, *Energy Environ. Sci.*, 2011, **4**, 675.
18 Y. J. Cui, J. S. Zhang, G. G. Zhang, J. H. Huang, P. Liu, a M. Antonietti and X. C. Wang, *J. Mater. Chem.*, 2011, **21**, 13032.
19 (*a*) X. X. Zou, G. D. Li, Y. N. Wang, J. Zhao, C. Yan, M. Y. Guo, L. Li and J. S. Chen, *Chem. Commun.*, 2011, **47**, 1066; (*b*) J. H. Liu, T. K. Zhang, Z. C. Wang, G. Dawson and W. Chen, *J. Mater. Chem.*, 2011, **21**, 14398; (*c*) F. Dong, L. W. Wu, Y. J. Sun, M. Fu, Zh. B. Wu and S. C. Lee, *J. Mater. Chem.*, 2011, **21**, 15171.
20 T. P. Ang and Y. M. Chan, *J. Phys. Chem. C*, 2011, **115**, 15965.
21 K. L. Kauffman, J. T. Culp, A. Goodman and C. Matranga, *J. Phys. Chem. C*, 2011, **115**, 1857.
22 M. Tabbal, T. Christidis, S. Isber, P. Merel, M. A. E. Khakani, M. Chaker, A. Amassian and L. Martinu, *J. Appl. Phys.*, 2005, **98**, 044310.
23 (*a*) F. Z. Su, S. C. Mathew, G. Lipner, X. Z. Fu, M. Antonietti, S. Blechert and X. C. Wang, *J. Am. Chem. Soc.*, 2010, **132**, 16299; (*b*) F. Z. Su, S. C. Mathew, L. Möhlmann, M. Antonietti, X. C. Wang and S. Blechert, *Angew. Chem., Int. Ed.*, 2011, **50**, 657; (*c*) Y. J. Cui, Z. X. Ding, P. Liu, M. Antonietti, X. Z. Fu and X. C. Wang, *Phys. Chem. Chem. Phys.*, 2012, **14**, 1455.